



## Radar observations of asteroid 1999 JM8

LANCE A. M. BENNER<sup>1\*</sup>, STEVEN J. OSTRO<sup>1</sup>, MICHAEL C. NOLAN<sup>2</sup>, JEAN-LUC MARGOT<sup>3</sup>,  
JON D. GIORGINI<sup>1</sup>, R. SCOTT HUDSON<sup>4</sup>, RAYMOND F. JURGENS<sup>1</sup>, MARTIN A. SLADE<sup>1</sup>, ELLEN S. HOWELL<sup>2</sup>,  
DONALD B. CAMPBELL<sup>5</sup> AND DONALD K. YEOMANS<sup>1</sup>

<sup>1</sup>Jet Propulsion Laboratory, California Institute of Technology, Pasadena, California 91109-8099, USA

<sup>2</sup>Arecibo Observatory, National Astronomy and Ionosphere Center, Arecibo, Puerto Rico 00612, USA

<sup>3</sup>Division of Geological and Planetary Sciences, California Institute of Technology, Pasadena, California 91125, USA

<sup>4</sup>School of Electrical Engineering and Computer Science, Washington State University, Pullman, Washington 99164-2752, USA

<sup>5</sup>National Astronomy and Ionosphere Center, Space Sciences Building, Cornell University, Ithaca, New York 14853, USA

\*Correspondence author's e-mail address: lance@reason.jpl.nasa.gov

(Received 2001 November 2; accepted in revised form 2002 February 5)

**Abstract**—We report results of delay-Doppler observations of 1999 JM8 with the Goldstone 8560 MHz (3.5 cm) and Arecibo 2380 MHz (13 cm) radars over 18 days in July–August 1999. The images place thousands of pixels on the asteroid and achieve range resolutions as fine as 15 m/pixel. The images reveal an asymmetric, irregularly shaped object with a typical overall dimension within 20% of 7 km. If we assume that 1999 JM8's effective diameter is 7 km, then the absolute magnitude, 15.15, and the average Goldstone radar cross section, 2.49 km<sup>2</sup>, correspond to optical and radar albedos of 0.02 and 0.06, establishing that 1999 JM8 is a dark object at optical and radar wavelengths. The asteroid is in a non-principal axis spin state that, although not yet well determined, has a dominant periodicity of ~7 days. However, images obtained between July 31 and August 9 show apparent regular rotation of features from day to day, suggesting that the rotation state is not far from principal axis rotation. 1999 JM8 has regions of pronounced topographic relief, prominent facets several kilometers in extent, numerous crater-like features between ~100 m and 1.5 km in diameter, and features whose structural nature is peculiar. Arecibo images provide the strongest evidence to date for a circular polarization ratio feature on any asteroid. Combined optical and radar observations from April 1990 to December 2000 permit computation of planetary close approach times to within ±10 days over the interval from 293 to at least 2907, one of the longest spans for any potentially hazardous asteroid. Integration of the orbit into the past and future shows close approaches to Earth, Mars, Ceres, and Vesta, but the probability of the object impacting Earth is zero for at least the next nine centuries.

### INTRODUCTION

1999 JM8 was discovered by LINEAR on 1999 May 13, fortuitously more than 2 months prior to an encounter within 0.057 AU (22 lunar distances) of Earth in July 1999, when it reached visual magnitude 14. It originally had been discovered at Palomar in April 1990 by E. F. Helin and designated 1990 HD1, but was lost. M. Hicks, B. Buratti, and M. Hanner (pers. comm.) obtained photometric colors, visible–infrared spectroscopy, and thermal infrared radiometry suggesting that 1999 JM8 is a C- or X-type (*i.e.*, E-, M-, or P-type) object; subsequent visible–infrared observations obtained by one of us (E. S. H.) at McDonald Observatory yielded a spectrum more consistent with an EMP-type object. Photometry obtained by L. Šarounová, P. Pravec, Y. Krugly, V. Shevchenko, S. Mottola, F. Lahulla, and M. Hicks (P. Pravec, pers. comm.) between July 3.0 and 21.9 indicated that 1999 JM8 is a very slow rotator. Pravec

*et al.* estimated a synodic rotation period of  $5.7 \pm 0.2$  days. The slow rotation period indicated that the echoes would be very strong and that observations on many days would be necessary to obtain thorough coverage in rotation phase. Consequently, prompt communication of the slow rotation period was invaluable for planning the radar observations. Table 1 summarizes the asteroid's optically-determined physical properties.

### OVERVIEW OF THE RADAR EXPERIMENT

The asteroid's close approach, large size, and extremely slow rotation provided an outstanding radar opportunity and we observed 1999 JM8 at Goldstone and Arecibo on 18 days between 1999 July 18 and August 9. Orbit solution JPL #15, used for the initial radar detection at Goldstone on July 18, was very good due to the 9 year arc of optical astrometry. Due to

TABLE 1. Optically-derived physical properties.

Property	Value	Reference*
$H$ (mag)	$15.15 \pm 0.10$	3
$G$	$-0.09 \pm 0.02$	3
Period (days)	$5.7 \pm 0.2$	3
$\Delta m$ (mag)	0.7	3
Taxonomy	C or EMP	1
	EMP	2

\*References: 1 = M. Hicks *et al.* (pers. comm.), 2 = E. S. Howell (pers. comm.), 3 = P. Pravec *et al.* (pers. comm.).

problems with the delay-Doppler data acquisition system, on July 18–19 we obtained only continuous wave (CW) (*i.e.*, Doppler-only) echoes. On July 20 we started with 2 CW transmit–receive cycles (runs), measured a Doppler correction, and then estimated the range with coarse-resolution 10 and 11  $\mu$ s (1500 and 1650 m resolution) setups. We completed that 70 min set of observations (track) with two imaging runs that resolved the target into about twenty 150 m range cells. We updated the orbit solutions several more times during the experiment; after July 20 range drift due to the ephemeris was imperceptible. Table 2 summarizes the Goldstone and Arecibo observations.

After July 20, our strategy during the Goldstone tracks was to do one or two CW runs to verify that we had echoes and

TABLE 2. Observations.

	Resolution ( $\mu$ s $\times$ Hz)	RA ( $^{\circ}$ )	DEC ( $^{\circ}$ )	$\Delta$ (AU)	Motion ( $^{\circ}$ )	OSOD	Runs	Start–Stop (HHMMSS–HHMMSS)
<b>Goldstone July 18</b>								
CW	0.977	187.6	59.7	0.100	0.04	15	1	211432–211609
CW	0.244					15	6	212119–213931
<b>Goldstone July 19</b>								
CW	0.061	186.5	60.0	0.098	0.54	15	10	014044–021542
CW	0.122					15	3	070604–071410
<b>Goldstone July 20</b>								
CW	0.244	182.5	63.5	0.093	0.12	17	2	023155–023633
	10 $\times$ 6.15					17	3	025009–025802
	11 $\times$ 2.24					17	1	030858–031029
	1 $\times$ 0.1					17	2	033703–034149
<b>Goldstone July 21</b>								
CW	0.244	173.4	63.5	0.084	0.14	19	1	174136–174257
	1 $\times$ 0.1					19	2	175851–180305
	1 $\times$ 0.1					19	14	180541–184433
<b>Goldstone July 23</b>								
CW	0.244	163.5	64.9	0.077	0.17	21	1	003648–003803
	0.5 $\times$ 0.075					21	4	005306–010223
	0.5 $\times$ 0.075					21	13	010410–013854
<b>Goldstone July 24</b>								
CW	0.244	146.0	65.5	0.070	0.60	21	2	165825–170154
	10 $\times$ 2.46					21	2	172513–172850
	11 $\times$ 2.24					21	2	174329–174659
	0.5 $\times$ 0.075					21	49	180151–195954
<b>Goldstone July 27</b>								
CW	0.244	118.4	62.0	0.062	0.35	21	2	013115–013422
	0.25 $\times$ 0.05					21	30	014947–025407
<b>Goldstone July 28</b>								
CW	0.244	101.4	55.6	0.058	0.51	23	1	171425–171514
	0.25 $\times$ 0.05					23	43	173023–190102
<b>Goldstone July 31</b>								
CW	0.244	81.7	38.7	0.058	0.85	23	2	170111–170404
	0.125 $\times$ 0.05					23	72	172454–195539
<b>Goldstone August 1</b>								
CW	0.244	78.3	33.9	0.059	1.10	23	2	120321–120617
	0.125 $\times$ 0.05					23	102	122101–155925
<b>Goldstone August 7</b>								
	0.25 $\times$ 0.075	64.1	6.2	0.082	0.11	26	16	171958–180409

TABLE 2. *Continued.*

	Resolution ( $\mu\text{s} \times \text{Hz}$ )	RA ( $^{\circ}$ )	DEC ( $^{\circ}$ )	$\Delta$ (AU)	Motion ( $^{\circ}$ )	OSOD	Runs	Start–Stop (HHMMSS–HHMMSS)
<b>Goldstone August 8</b>								
	$0.25 \times 0.075$	63.0	3.5	0.087	0.93	26	145	115342–191931
<b>Arecibo August 1</b>								
	4.0	78.4	34.1	0.059	0.34	21	2	123730–124051
	$0.1 \times 0.0098$					21	26	125104–135333
<b>Arecibo August 2</b>								
CW	–	74.9	28.4	0.061	0.34	23	1	123810–123903
	$0.1 \times 0.0094$					23	28	130204–135658
<b>Arecibo August 3</b>								
CW	–	72.0	23.2	0.064	0.36	23	2	121929–122235
	$0.1 \times 0.0089$					23	31	124312–134900
<b>Arecibo August 4</b>								
	$0.1 \times 0.0083$	69.5	18.3	0.068	0.04	23	5	132600–133504
<b>Arecibo August 5</b>								
CW	–	67.6	14.1	0.072	0.26	26	1	115436–115540
	$0.1 \times 0.0078$					26	35	115814–131950
<b>Arecibo August 6</b>								
	$0.1 \times 0.0074$	65.9	10.2	0.076	0.08	26	13	123350–130414
<b>Arecibo August 9</b>								
	$0.1 \times 0.0060$	62.1	1.3	0.091	0.14	26	25	104635–115923

Right ascension (RA), declination (DEC), and geocentric distance ( $\Delta$ ) are given at the mid-epoch of each day's observations. Motion indicates the plane-of-sky motion during each track. OSOD refers to the orbit solution computed using the JPL On-Site Orbit Determination software. Runs are the number of transmit–receive cycles with each setup. Start and stop refer to the UTC epochs at the beginning and end of reception of echoes.

then devote the rest of the track to the finest resolution imaging permitted by the signal-to-noise ratio. For the final Goldstone tracks on August 7 and 8, the asteroid was  $\sim 50\%$  farther away than at the closest approach, so we used a coarser resolution of  $0.25 \mu\text{s} \times 0.075 \text{ Hz}$ . However, this still placed thousands of pixels on the target.

At Arecibo we used two imaging data acquisition systems: the Caltech Baseband Recorder (CBR), which was designed for observing pulsars and was made available to us by Stuart Anderson, and a new system (the Portable Fast Sampler, or PFS) that was then under development. We used both systems on each day, but the analyses reported here utilize the CBR data exclusively due to the modestly stronger signal-to-noise ratio and the CBR's dual-polarization capability. The range resolution on all days was 15 m and the frequency resolution varied from 0.010 to 0.006 Hz depending on the date (Table 2).

#### ASTROMETRY AND ORBIT REFINEMENT

Table 3 lists 1999 JM8 radar astrometry and best-fit residuals for a post-experiment orbit solution and Table 4 lists the estimated orbital elements and their uncertainties. Combined optical and radar observations from April 1990 to December 2000 permit reliable computation of the orbit over the interval from 293 to at least 2907, one of the longest spans

for any near-Earth asteroid (NEA). Here "reliable" means that the  $3\sigma$  uncertainty in the epochs of close approaches is  $< 10$  days.

Table 5 shows approaches within 0.1 AU of Earth, Mars, Ceres, and Vesta and within 1.0 AU of Jupiter during that interval. There have been multiple encounters with Earth, Mars, Ceres, Vesta, and Jupiter in the past, but in the next millennium all the encounters are with Earth, none closer than that in 1999. The impact probability through 2907 is effectively zero.

#### DISC-INTEGRATED PROPERTIES

Our methods of radar data reduction and analysis follow those described in detail by Ostro *et al.* (1992, 1996). In Doppler-only observations, echoes were received simultaneously in the opposite (OC) and same (SC) senses of circular polarization as the transmission.  $\sigma_{OC}$  is the OC radar cross section; uncertainties in  $\sigma_{OC}$  are dominated by systematic pointing and calibration errors that are typically between 20 and 50%. The circular polarization ratio SC/OC is a gauge of near-surface roughness at spatial scales within about an order of magnitude of the radar wavelength (12.6 cm at Arecibo and 3.53 cm at Goldstone). For SC/OC, systematic effects cancel and most remaining statistical errors propagate from receiver thermal noise.

Table 6 summarizes 1999 JM8's 3.5 cm disc-integrated properties and Fig. 1 shows a collage of CW spectra obtained

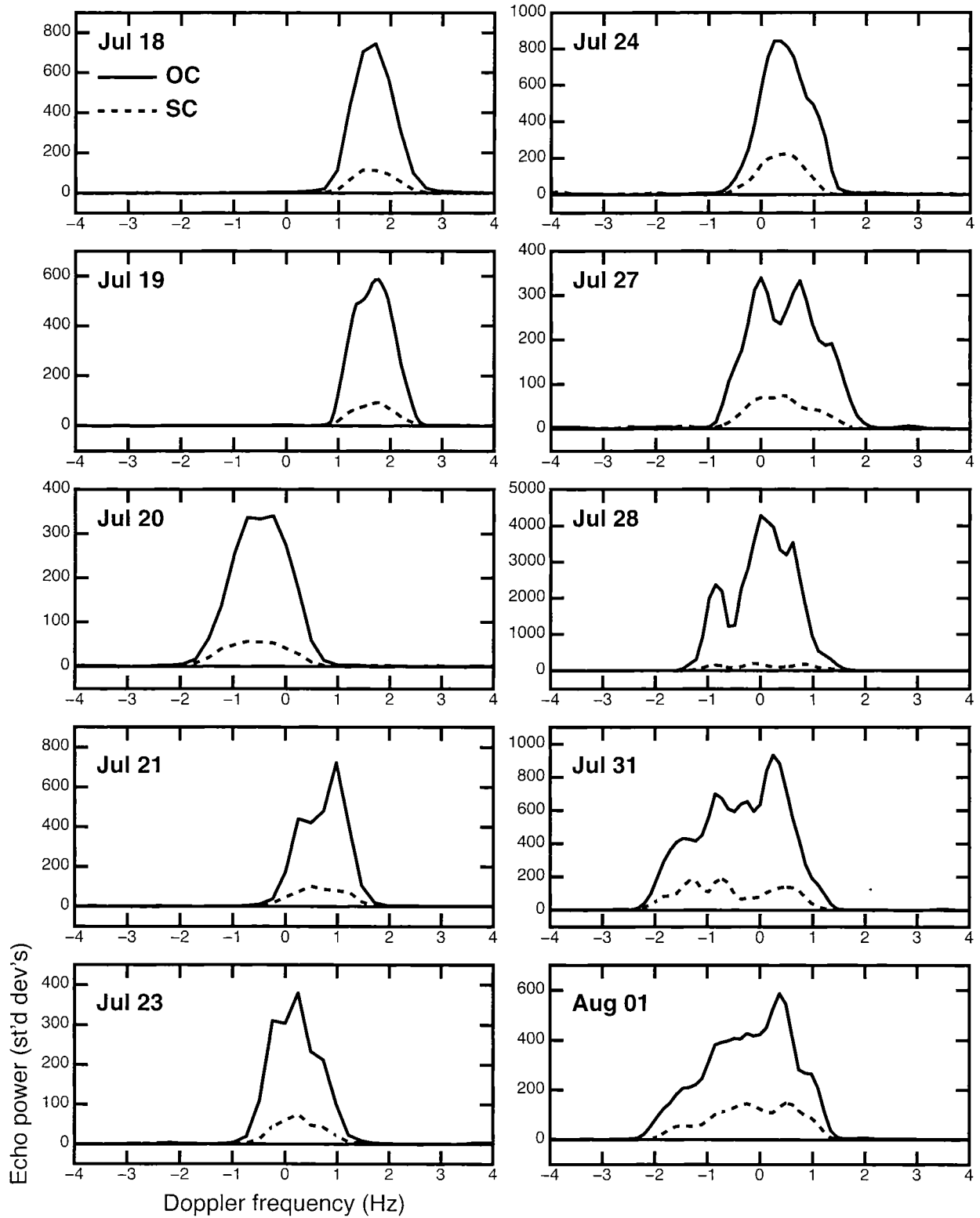


FIG. 1. Weighted sums of Goldstone echo power spectra grouped by observation date between July 18 (top left) to August 1 (bottom right). The spectra have been smoothed to a resolution of 0.5 Hz.

TABLE 3. Radar astrometry.

UTC epoch	OSOD Solution	Correction	Measurement	$\pm$	Residual
1999 07 18 21:30:00	15	+1.7 Hz	580912.4 Hz	0.4 Hz	0.175
1999 07 20 02:40:00	17	-0.5 Hz	547278.4 Hz	0.3 Hz	0.125
1999 07 20 03:00:00	17	-3132.5 $\mu$ s	92.6270694 s	10.0 $\mu$ s	-2.215
1999 07 21 17:40:00	19	+0.8 Hz	528308.3 Hz	0.4 Hz	0.439
1999 07 24 17:00:00	21	+0.5 Hz	420950.7 Hz	0.3 Hz	0.163
1999 07 24 19:00:00	21	-4 $\mu$ s	69.426792 s	5.0 $\mu$ s	2.538
1999 07 27 01:30:00	21	+0.5 Hz	264385.7 Hz	0.3 Hz	-0.272
1999 07 27 02:30:00	21	-20 $\mu$ s	61.40113 s	5.0 $\mu$ s	-1.574

Astrometry corresponds to echoes from 1999 JM8's estimated center of mass. The reference point for Goldstone is the intersection of the altitude and azimuth axes of the 70 m antenna, DSS-14. Residuals are the remaining difference when the best-fit prediction of solution #34 is subtracted from the actual measurements. The range equivalent of 1  $\mu$ s is 150 m and the radial velocity equivalents of 1 Hz are 17.6 mm/s at Goldstone's transmitter frequency of 8560 MHz.

TABLE 4. Orbit.

Quantity	Value	Uncertainty
Epoch	2451911.5 JD (= 2001 January 02.0)	
Eccentricity ( $e$ )	0.64440537378	$\pm 0.0000000086$
Perihelion distance ( $q$ )	0.96733323427 AU	$\pm 0.0000000156$ AU
Perihelion date ( $T_p$ )	2451383.7257358508 JD (1999 July 24.22574)	$\pm 0.0000052119$ day
Long. asc. node ( $\Omega$ )	134.00962375234°	$\pm 0.0000052995^\circ$
Arg. of perihelion ( $\omega$ )	165.98932252768°	$\pm 0.0000095614^\circ$
Inclination ( $i$ )	13.7134598550°	$\pm 0.0000029247^\circ$
Semimajor axis ( $a$ )	2.72032579502 AU	$\pm 0.0000000472$ AU
Period	1638.81453203005 days (4.48675103853089 years)	$\pm 0.00004263$ day
Mean anomaly	115.93669166356°	$\pm 0.0000030143^\circ$

1999 JM8's heliocentric orbital elements (OSOD solution #34) and formal 1-standard deviation uncertainties, estimated using our delay-Doppler radar astrometry (Table 3) and currently available optical astrometry (403 angular measurements from 1990 April 29 to 2000 December 31). The mean post-fit radar residuals are: time-delay  $-0.417 \pm 2.57 \mu$ s, and Doppler frequency,  $+0.125 \pm 0.255$  Hz. Mean post-fit optical residuals are RA,  $-0.02 \pm 0.54''$ , and declination,  $-0.03 \pm 0.63''$ . The r.m.s. of residuals normalized by the assigned measurement uncertainty are (0.368, 0.732, 0.589) for delay data, Doppler data, and total data set (including optical), respectively. Elements are in the coordinate frame of the JPL planetary ephemeris DE405 (ICRF93/ J2000, a quasar-based radio frame, generally within 0.01 arcseconds of the optical FK5/J2000 frame). Angular elements are referred to the ecliptic and mean equinox of J2000.

at Goldstone on each day. The 3.5 cm cross section varies significantly from day-to-day and we obtain an average of 2.49 km<sup>2</sup>, to which we assign an uncertainty of 35%. During the course of the experiment the bandwidths increased from  $\sim 1.5$  to 3.4 Hz, suggesting a more equatorial view on later dates and/or an irregular shape. 1999 JM8's average SC/OC =  $0.19 \pm 0.01$  is less than the median of  $\sim 0.28$  estimated for all radar-detected NEAs, so the the object's near-surface roughness is somewhat less than average.

## DELAY-DOPPLER IMAGES

Figure 2 shows a chronological sequence of OC delay-Doppler images obtained between July 20 and August 9. Each frame has the same range and radial velocity dimensions. Most of the images are sums of all the highest resolution runs on each day. Due to the well-known north-south ambiguity inherent in delay-Doppler images, we do not know in which hemisphere individual features occur.

TABLE 5. Close approaches.

Date	Body	Close-approach distance			$V_{\text{rel}}$ (km/s)	$\Delta T$ (min)	Nsig
		Nominal (AU)	Min (AU)	Max (AU)			
293 Sep 19.76	Jupiter	0.9235	0.9009	0.9460	5.7	5079	$3.4 \times 10^6$
412 May 24.48	Jupiter	0.9636	0.9523	0.9748	6.0	3783	$1.5 \times 10^6$
507 May 4.44	Jupiter	0.9576	0.9370	0.9779	5.6	4290	$7.4 \times 10^5$
584 May 11.34	Earth	0.0599	0.0437	0.0812	13.3	6516	$5.9 \times 10^4$
625 Dec 22.81	Jupiter	0.9933	0.9837	0.0029	6.0	2621	$1.7 \times 10^6$
756 Aug 1.34	Jupiter	0.9963	0.9788	0.0136	5.7	2641	$5.9 \times 10^5$
811 May 11.51	Earth	0.0591	0.0340	0.0881	13.1	6987	$2.2 \times 10^5$
1024 Nov 22.16	Mars	0.0591	0.0591	0.0621	15.1	2211	$3.3 \times 10^5$
1060 May 10.83	Earth	0.0867	0.0864	0.0887	13.9	2974	$9.2 \times 10^5$
1078 Jun 7.22	Mars	0.0510	0.0384	0.0641	14.4	1507	$6.0 \times 10^4$
1091 Aug 18.89	Earth	0.0794	0.0759	0.0833	14.4	1039	$3.5 \times 10^5$
1105 Aug 28.53	Ceres	0.0883	0.0881	0.0885	14.1	58	$3.2 \times 10^4$
1123 Jul 1.11	Vesta	0.0814	0.0770	0.0857	12.6	353	$5.9 \times 10^4$
1194 Aug 24.21	Earth	0.0462	0.0454	0.0470	15.0	214	$1.7 \times 10^5$
1256 Mar 23.79	Mars	0.0692	0.0658	0.0728	16.1	462	$1.6 \times 10^5$
1261 Jun 18.77	Vesta	0.0771	0.0757	0.0785	13.7	275	$1.7 \times 10^5$
1269 Jun 4.02	Mars	0.0701	0.0690	0.0712	14.5	319	$2.0 \times 10^5$
1318 May 3.59	Mars	0.0919	0.0914	0.0926	14.4	565	$4.4 \times 10^5$
1412 Aug 25.85	Earth	0.0459	0.0455	0.0463	15.1	54	$1.3 \times 10^4$
1474 Aug 21.81	Earth	0.0546	0.0545	0.0547	14.0	22	$1.9 \times 10^5$
1692 Aug 9.95	Earth	0.0963	0.0963	0.0964	13.4	15	$7.6 \times 10^5$
1981 Aug 20.29	Earth	0.0665	0.0665	0.0665	13.8	6	$5.6 \times 10^5$
1990 Aug 8.41	Earth	0.0335	0.0335	0.0335	12.7	2	$6.5 \times 10^5$
1999 Jul 30.40	Earth	0.0568	0.0568	0.0568	12.3	0	$5.4 \times 10^6$
2137 Aug 1.53	Earth	0.0764	0.0764	0.0764	13.3	6	$1.5 \times 10^6$
2573 Aug 11.86	Earth	0.0852	0.0852	0.0852	14.0	5	$8.6 \times 10^5$
2791 Aug 15.18	Earth	0.0947	0.0947	0.0947	14.0	15	$4.3 \times 10^5$
2831 Jul 26.37	Earth	0.0715	0.0715	0.0715	14.0	12	$2.4 \times 10^5$
2907 Jul 20.53	Earth	0.0911	0.0911	0.0911	14.2	3	$6.9 \times 10^4$

Note: Close approaches within 0.1 AU of the given body except for Jupiter, which is indicated for approaches  $<1.0$  AU, are listed along with nominal,  $3\sigma$  minimum and maximum distances.  $V_{\text{rel}}$  is the relative velocity at the nominal close approach,  $\Delta T$  is the  $3\sigma$  uncertainty in the epoch of close approach, and Nsig is the number of standard deviations required for the uncertainty ellipse to intersect the close-approach body.

Table 7 gives the asteroid's visible range extents and bandwidths measured from the images on each day. The maximum extents are 5.3 km on August 6 and 3.6 Hz (when adjusted to Goldstone's transmitter frequency of 8560 MHz) on August 5. The Arecibo images generally show larger range extents than the Goldstone images, perhaps due to the greater sensitivity at Arecibo and/or to differences in the asteroid's orientation. On August 1, the only day of overlap between the two observatories, the visible range extent in the Arecibo image is  $\sim 0.3$  km deeper. The images have an average visible range extent of 3.6 km. Based on our experience with shape inversions of other objects, the visible range extent typically is about one-half of the true range extent; if so, then 1999 JM8's true range extent is  $\sim 7$  km.

Prominent features in the images appear to rotate by  $\sim 50^\circ$  from day-to-day between July 31 and August 9, suggesting that

1999 JM8 has an apparent rotation period of  $\sim 1$  week and that the subradar latitude was within a few tens of degrees of zero during that interval. Images obtained on July 24, August 1, and August 8 show very similar surface features, suggesting that the rotation phases were nearly the same and offering additional support for an apparent rotation period of  $\sim 7$  days. We searched for evidence of rotation among images obtained on the same day and found it on several days (*e.g.*, on August 5 and 8, the longest Arecibo and Goldstone tracks; Fig. 3) at rates consistent with the rotation seen from day to day.

The rotation period evident in the delay-Doppler images is somewhat longer than the 5.7 day estimate obtained by Pravec *et al.* The difference could be due to the effects of the large solar phase angles between  $85$  and  $120^\circ$  on dates when the lightcurves were obtained (1999 July 3–21) and the asteroid's irregular shape, sky motion, and the rotation state (which is

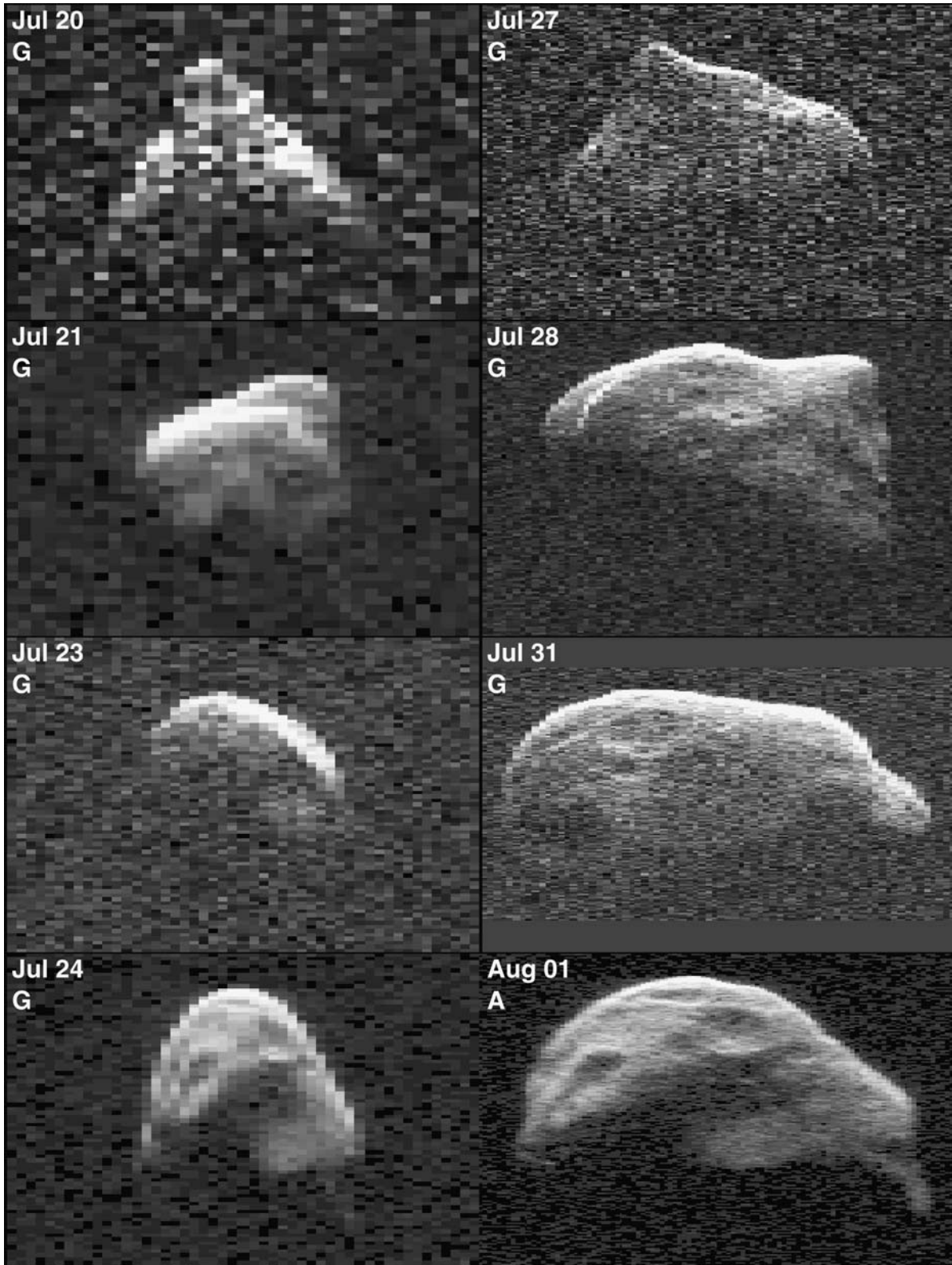


FIG. 2. Sequence of OC delay-Doppler images obtained at Goldstone and Arecibo. In each image range increases from top to bottom and Doppler frequency increases from right to left, so rotation is clockwise. The height in each frame is 6.0 km ( $40 \mu\text{s}$ ). The images are shown with a Doppler extent of 3.7 Hz when adjusted to a transmitter frequency of 8560 MHz in order to facilitate direct comparison between Goldstone and Arecibo images. The images have logarithmic contrast stretches in order to take advantage of the dynamic range. The collage shows one image per day, where each frame is the sum of all the highest resolution images on a given day. On August 1 we imaged 1999 JM8 at both telescopes; the image shown was obtained at Arecibo. "A" and "G" indicate images obtained at Arecibo and Goldstone, respectively. *Figure is continued on the next page.*

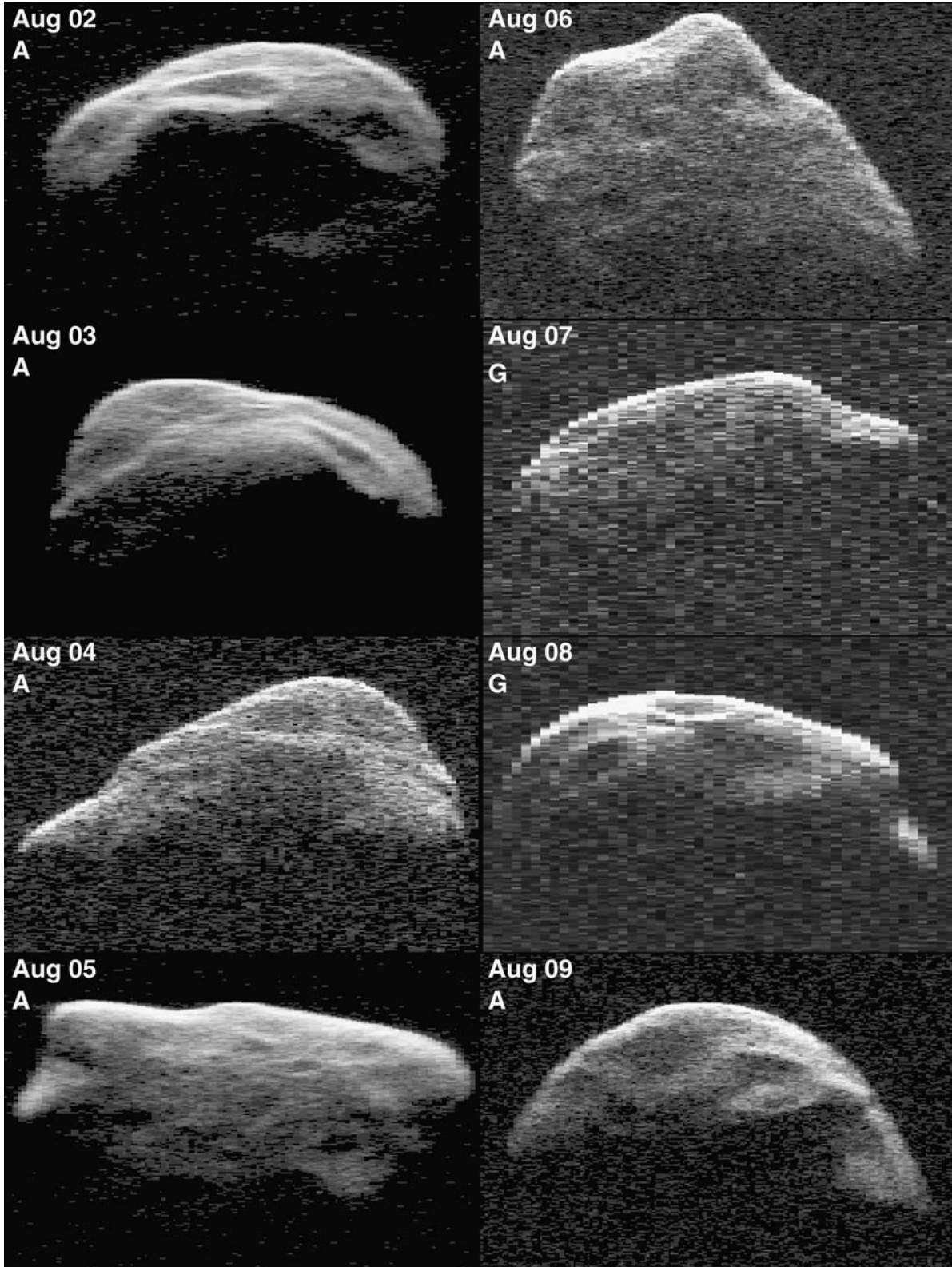


FIG. 2. *Continued.*

TABLE 6. Disc-integrated 3.5 cm radar properties.

Date	Runs	FFTs	OC SNR	$B$ (Hz)	$\sigma_{OC}$ (km <sup>2</sup> )	SC/OC ( $\pm 0.01$ )
Jul 18	7	1270	940	1.5	2.96	0.19
Jul 19	10	1576	540	1.3	2.46	0.21
Jul 20	2	154	500	2.0	2.97	0.19
Jul 21	1	140	830	1.7	3.54	0.22
Jul 23	1	132	580	1.6	2.26	0.16
Jul 24	2	162	1100	2.3	2.85	0.15
Jul 27	2	216	520	2.6	1.08	0.18
Jul 28	1	80	5700	2.9	3.02	0.17
Jul 31	2	180	1400	3.3	1.94	0.22
Aug 1	2	192	880	3.4	1.81	0.23
Experiment average					2.49	0.19

The bandwidths were estimated using CW spectra with a resolution of 0.122 Hz.  $B$  is the echo bandwidth. The cross sections and SC/OC were estimated using a frequency resolution of 1.95 Hz in order to have enough fast-Fourier transforms (FFTs) to approach Gaussian noise statistics. SNR = signal-to-noise

TABLE 7. Delay-Doppler dispersions.

Date	Resolution ( $\mu s \times Hz$ )	Delay extent (km)	Bandwidth (Hz)
<b>Goldstone (3.5 cm)</b>			
Jul 19	CW 0.061	no data	1.3
Jul 20	$1.0 \times 0.1$	2.85	1.8
Jul 21	$1.0 \times 0.1$	2.70	1.6
Jul 23	$0.5 \times 0.075$	2.55	1.43
Jul 24	$0.5 \times 0.075$	4.28	1.65
Jul 27	$0.25 \times 0.05$	3.26	2.40
Jul 28	$0.25 \times 0.05$	3.90	2.65
Jul 31	$0.125 \times 0.05$	3.45	3.35
Aug 1	$0.125 \times 0.05$	4.16	3.05
Aug 7	$0.25 \times 0.075$	2.66	3.15
Aug 8	$0.25 \times 0.075$	3.30	3.38
<b>Arecibo (12.6 cm)</b>			
Aug 1	$0.1 \times 0.0098$	4.50	3.31
Aug 2	$0.1 \times 0.0094$	4.13	3.17
Aug 3	$0.1 \times 0.0089$	3.71	3.17
Aug 4	$0.1 \times 0.0083$	3.47	3.24
Aug 5	$0.1 \times 0.0078$	4.32	3.63
Aug 6	$0.1 \times 0.0074$	5.27	3.20
Aug 9	$0.1 \times 0.0060$	3.96	3.34

Estimated dispersions include pixels with echo power above the  $2\sigma$  level, except on July 27, 28, and 31, when contiguous pixels with signal-to-noise ratios  $> 1.0$  were used. July 24 and August 1 estimates include the distant arc of pixels at the trailing edge that Arecibo images indicate are real. Arecibo bandwidths have been multiplied by 8560/2380 (the ratio of the Goldstone and Arecibo transmitter frequencies) to facilitate comparison with 3.5 cm results.

discussed below). Given that we can see rotation directly in the delay-Doppler images, in the analysis below we adopt a rotation period of 7 days as our nominal rotation period estimate. A more precise estimate of the spin state will require inversion of the delay-Doppler images and lightcurves.

Because the July 31 to August 9 image sequence is strikingly similar to what we would expect for a principal axis rotator viewed close to its equatorial plane, we adjusted the images to the same delay and Doppler scales and aligned them by hand to construct an estimate of 1999 JM8's pole-on silhouette (Fig. 4). The silhouette's elongation is  $\sim 1.15$ , a value that ranks near the lower end of the distribution of radar-derived NEA elongations, which have a mean and root mean square (rms) dispersion of  $1.6 \pm 0.4$  (Ostro *et al.* 2001).

### SPIN STATE

Is 1999 JM8's rotation principal axis (PA) or non-principal axis (NPA)? Let us pretend that it is principal axis and then examine the images to see if this assumption is valid. The apparent rotation vector  $W_{app}$  is the vector sum of the intrinsic rotation  $W_{int}$  and the contribution due to sky motion  $W_{sky}$ . Figure 5 shows that the sky motion varied from a minimum of  $\sim 2^\circ$  per day to a maximum of  $\sim 7^\circ$  per day. Between July 20 and 28, the appearance of the asteroid changed substantially from day to day (it is difficult to identify the same features on adjacent days), indicating considerable apparent daily rotation. Between July 31 and August 9 we observe  $\sim 50^\circ$  of rotation per day, so  $W_{int}$  dominates  $W_{sky}$ , and  $W_{app} \approx W_{int}$ .

Delay-Doppler images obtained on July 24 and August 1, days in which the sky motion was  $\sim 4^\circ$  and  $7^\circ$ , have very similar orientations but their bandwidths differ by about a factor of 2:



FIG. 3. Difference images obtained on August 5 (left) and 8 (right), the longest tracks at Arecibo and Goldstone. Range increases from top to bottom and Doppler frequency increases from right to left, so rotation is clockwise. The August 5 (Arecibo) image shows the difference between the first (white) and last (black) runs on that day, which were obtained 1.3 h apart. The August 8 (Goldstone) image shows the difference between the first 17 runs (white) and the last 14 runs (black), which were obtained 7.5 h apart. Several degrees of rotation are evident in the August 8 image.

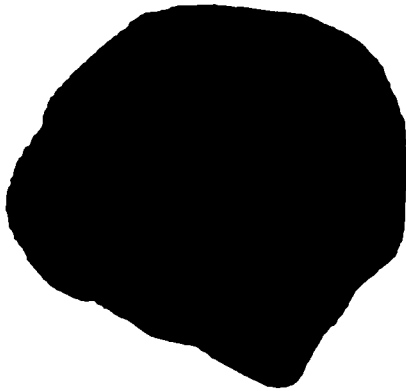


FIG. 4. Silhouette of 1999 JM8 using delay-Doppler images obtained between August 1 and 9 assuming principal axis rotation. Images were cut out from hardcopies and aligned by eye.

$$\begin{aligned} B_{\text{Jul24}}/B_{\text{Aug1}} &= B_1/B_2 \\ &= (1.7 \pm 0.15 \text{ Hz})/(3.3 \pm 0.15 \text{ Hz}) \\ &= 0.52 \pm 0.05 \end{aligned}$$

If the spin is PA, this bandwidth change was due to the change in subradar latitude  $\delta$  from July 24 to August 1. Expressing the apparent rotation period  $P$  in hours and the diameter  $D$  in kilometers gives the 8560 MHz bandwidth  $B$

in hertz:  $B = 100 D \cos \delta/P$ , so the ratio of the bandwidths  $B_1/B_2 = \cos \delta_1/\cos \delta_2 = 0.52$  could be caused by a change in  $\cos \delta$  due to the  $\sim 50^\circ$  of sky motion between the 2 days. Furthermore,  $|\delta_2| \geq 0^\circ$  and  $|\cos \delta_2| \leq 1$ , so  $|\cos \delta_1| \leq 0.52$  and  $|\delta_1| \geq 59^\circ$ .

However, visual inspection of features in the July 24 and August 1 images suggests that the orientations of 1999 JM8 on those days differ by  $<10^\circ$  of latitude. To quantify the latitude difference  $|\delta_1 - \delta_2|$ , we measured the locations in range relative to the leading edge of several features that are visible in images on both July 24 and August 1. The features differ in range by  $\sim 0.5$  to  $\sim 1 \mu\text{s}$ , which is 1–2 range pixels at the July 24 resolution, indicating that the displacement in latitude is small. We quantified the displacement further by computing the latitude difference that is implied by 0.15 km ( $1 \mu\text{s}$ ) of displacement on a sphere  $\sim 7$  km in diameter. We are convinced that  $10^\circ$  is a conservative number unless the subradar latitude on July 24 was within a few degrees of the pole, which is impossible because that would imply an object larger by a factor of several than the one observed.

Let us adopt the upper limit on the change in  $|\delta_1 - \delta_2|$  of  $10^\circ$  and explore its implications:

First	$\cos \delta_1 = (0.52) \cos \delta_2$
Then	$\cos(\delta_2 + 10^\circ) = (0.52) \cos \delta_2$

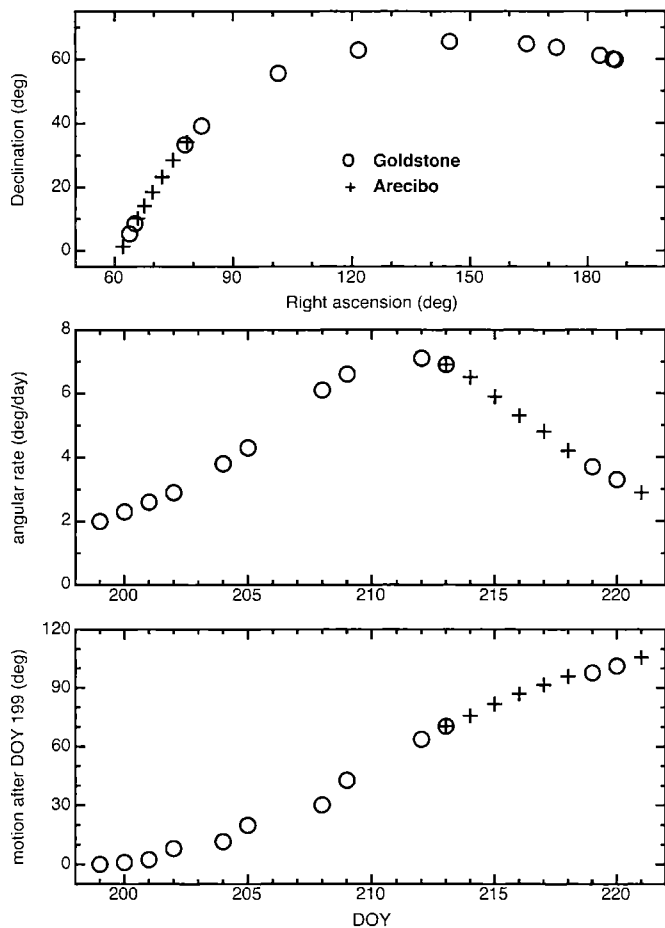


FIG. 5. (Top) Right ascension and declination of 1999 JM8 at the mid epoch of each track. Observations at Goldstone and Arecibo are indicated with circles and crosses. (Middle) Angular rate of sky motion as a function of day-of-year (DOY). (Bottom) Angular separation of 1999 JM8 as a function of DOY relative to the first Goldstone track on DOY 199 (July 18).

After applying a trigonometry identity and some algebra we obtain:

$$\sin \delta_2 / \cos \delta_2 = \tan \delta_2 = (\cos 10^\circ - 0.52) / \sin 10^\circ$$

So  $\delta_2 = 69.5^\circ$

Therefore:  $\delta_1 = \delta_2 + 10^\circ = 79.5^\circ$

That is, principal axis (PA) rotation requires that the subradar latitude had an absolute value of at least  $79.5^\circ$  on July 24. If  $|\delta_1| \geq 79.5^\circ$  on July 24, then the  $\sim 7$  day rotation period evident in the images and the bandwidth of 1.7 Hz constrains the diameter:

$$D \geq (1.7 \text{ Hz})(\sim 7 \text{ days})(24 \text{ h/day}) / (100 \cos 79.5^\circ)$$

$$D \geq 15.7 \text{ km}$$

However, the visible range extents, which presumably show about one-half of the true range extent, average only 3.6 km (Table 7), which is inconsistent with  $D \geq 15.7$  km. Thus, the assumption of PA rotation leads to a contradiction and we are forced to conclude that 1999 JM8 is a non-principal axis (NPA) rotator.

We also conducted a search for PA spin states in which sky motion was explicitly included. We searched for spin state/diameter combinations that match the observed bandwidths and produce similar longitudes on July 24, August 1, and August 8, days when the orientation of 1999 JM8 is very similar. The search covered the entire sky at  $5^\circ$  intervals, rotation periods between 5.0 and 18.0 days at intervals of 0.1 days, diameters between 3.5 and 10.0 km in 0.1 km increments, and the search assumed that 1999 JM8 is spherical.

We found that PA spin states fit the observations only if the absolute values of the subradar latitudes are about  $55\text{--}63^\circ$  on July 24, about  $15\text{--}25^\circ$  on August 1, and  $5\text{--}15^\circ$  (and on the opposite side of the equator relative to the other 2 days) on August 8. That is, in order for principal axis rotation to fit the observations, the subradar latitudes on July 24 and August 1 must differ by  $30\text{--}40^\circ$ . However, that contradicts the striking similarities seen in the images, which indicate a latitude difference on those days of much  $<30^\circ$ .

Stated more succinctly, the July 24 and August 1 images clearly show the same side of 1999 JM8 but have bandwidths that differ by nearly a factor of 2. Given that  $W_{\text{int}}$  dominates over  $W_{\text{sky}}$ , the position of the spin vector in the asteroid had to be different on the 2 days; that is, the spin must be NPA. On the other hand, the apparent regular rotation of features in images between July 31 and August 1 suggests that  $W_{\text{int}}$  has a period of  $\sim 1$  week and that the rotation state is not far from PA rotation. PA rotation would be admissible if the latitude difference between July 24 and August 1 was  $30\text{--}40^\circ$ , so the upper bound of  $10^\circ$  on the difference in latitudes suggests that the spin axis moved by at least  $20^\circ$  in 7 days. Refined estimates of the spin state will require shape inversion, which is beyond the scope of this paper.

Several other slowly rotating asteroids are suspected of being NPA rotators. 4179 Toutatis is in a well-defined NPA state (Hudson and Ostro, 1995) and NPA rotation is strongly suspected for 253 Mathilde (Mottola *et al.*, 1995), 288 Glauke (Harris *et al.*, 1999), 3288 Seleucus (Harris *et al.*, 1999), 4486 Mithra (Ostro *et al.*, 2000), and 38071 (1999 GU3) (Pravec *et al.*, 2000).

### SURFACE FEATURES

The sequence of daily images from July 31 to August 9 show a clear progression of familiar prominent features. 1999 JM8 has an irregular, asymmetric shape characterized by regions of pronounced topographic relief, prominent facets several kilometers in extent, at least one large concavity, and numerous

smaller concavities. On July 23, 24, August 1, 2, 8, and 9, the leading edge is rounded. In contrast, on July 20, 27, 28, August 5, and 6, the leading edge is more angular and the July 20 image is almost triangular.

On several days the leading edges show relative topographic relief of up to several hundreds of meters. For example, the July 27 leading edge shows a pronounced "peak" extending  $\sim 400$  m toward the radar. The July 28 leading edge has a "valley" that is 100–300 m more distant in range than the two adjacent "hills".

There is a large, nearly flat feature evident on the leading edges of the July 31 and August 1 images. On July 31 the feature extends across the middle of the leading edge and on August 1 it is on the right (receding side), with a range extent of at least 2 km. The August 4–6 images show a prominent, nearly flat region on the leading edge that, as seen in the August 6 image, has a range extent of at least 5 km.

A prominent relatively dark feature, apparently a 2 km diameter concavity, is near the center of the trailing edge on July 24, August 1, 2, 8, and 9. It is the largest concavity evident in the images.

Other circular to ellipsoidal and relatively dark features are probably impact craters; they have diameters ranging from  $\sim 100$  m to  $\sim 1$  km. One of the smallest, near the center of the July 28 image, is surrounded by a relatively bright annulus that is reminiscent of the relatively bright ejecta deposits seen near impact craters in Arecibo delay-Doppler images of the Moon (Thompson *et al.*, 1981) and Venus (Campbell *et al.*, 1990). Two large, kilometer-sized crater-like structures are particularly prominent on July 24, 31, August 1, 2, and 8.

### POLARIZATION SIGNATURE

Figure 6 shows daily sums of SC, OC, and SC/OC images obtained at Arecibo. The images show only those pixels in which the echo power in both polarizations exceeds 3-standard deviations. Each ratio image shows a region of relatively low SC/OC  $\approx 0.1$  at the echo's leading edge and a general pattern of increasing SC/OC (to  $\geq 0.5$ ) as a function of increasing range toward the trailing edge. This pattern is similar to that seen in SC/OC images from Toutatis (Ostro *et al.*, 1999). Low SC/OC at the leading edge reveals a smooth, specularly reflecting surface that preferentially returns OC echo near normal incidence. We also investigated thresholds of 5 and 10 standard deviations and found that although the number of points decreases with each increase in the threshold, the patterns in the distribution of SC/OC do not change significantly.

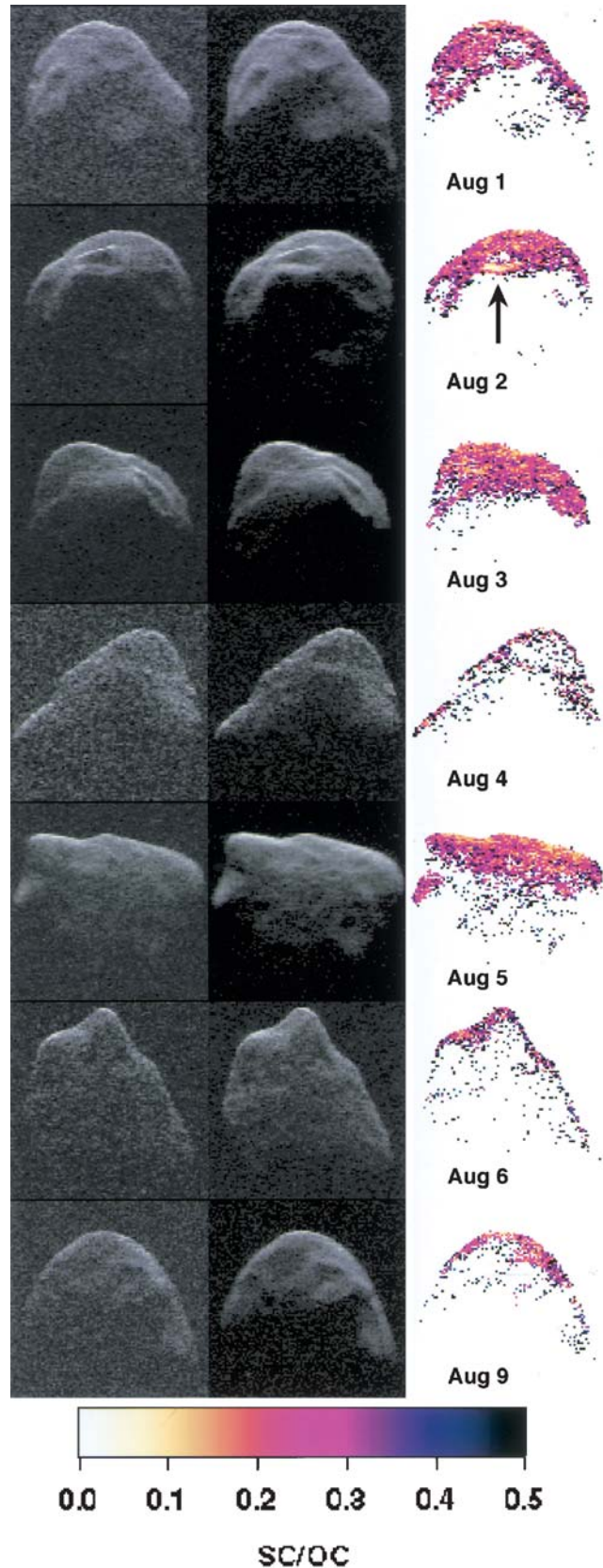


FIG. 6. (right) Arecibo SC (left), OC (middle), and SC/OC (right) images. The delay-Doppler extents and orientations are the same as in Fig. 2. SC/OC is plotted by adopting a detection threshold per pixel of  $3\sigma$  in both SC and OC images. All other pixels are mapped to white. The color stretch is saturated at SC/OC = 0.5 (black) in order to emphasize the most interesting regions of the dynamical range. An arrow points to a region with relatively low SC/OC on August 2.

Near the trailing edge of the August 2 image is an ellipsoidal region of  $\sim 200$  pixels with lower SC/OC than its surroundings. We filtered the image with a  $10 \times 10$  pixel boxcar and found that  $SC/OC = 0.08 \pm 0.01$  within the region and  $0.24 \pm 0.01$  at more positive and negative Doppler frequencies in the same span of range gates. The ellipsoidal structure is within an oval region that is relatively bright in both the SC and OC images. Its origin is not clear, and due to the north-south ambiguity, it is possible that there are contributions to the SC/OC difference from both hemispheres. One plausible explanation is that this may be a crater wall oriented at a low incidence angle that gives more specular reflections than adjacent regions. This may be evidence for a polarization ratio feature, which, if true, would be the first observed on an asteroid. There are also suggestions of narrow regions of lower SC/OC on August 1, 2, 3, and 5 adjacent to arcuate features that may be crater rims.

## DISCUSSION

If, as we suspect, 1999 JM8's effective diameter is  $\sim 7$  km, then the absolute magnitude of 15.15 (Table 1) corresponds to a very low optical geometric albedo  $p_v = 0.02$ . This albedo and the optical spectrum strongly suggest that 1999 JM8 is a P-class object. The average Goldstone radar cross section,  $2.49 \text{ km}^2$ , corresponds to a radar albedo of 0.06, an estimate that overlaps the radar albedos for C-, S-, and BFGP-type main-belt and near-Earth asteroids (Magri *et al.*, 1999).

How did the NPA rotation originate? Perhaps 1999 JM8 is a collisional fragment that was excited into NPA rotation during its dispersal from a larger progenitor, either directly into an NPA rotation state (Giblin and Farinella, 1997; Asphaug and Scheeres, 1999) or due to gravitational interactions with other fragments and/or the parent body (Scheeres *et al.*, 2000). Alternatively, perhaps the NPA rotation was caused by an impact into the asteroid or by gravitational torques during one or more very close passes by Earth or another planet (Scheeres *et al.*, 2000). The presence of at least 3 km sized concavities that appear to be impact craters is consistent with the hypothesis that the NPA rotation was induced by impacts, but the concavities do not rule out the other mechanisms. Perhaps a combination of these mechanisms is responsible.

Another viable explanation is that the NPA rotation could be the result of (or was modified by) outgassing if 1999 JM8 was once a comet. There is a precedent for this conjecture: comet Halley, which is known to be an NPA rotator (Belton, 1990; Belton *et al.*, 1991). 1999 JM8's timescale for damping to PA rotation (Harris, 1994) exceeds the age of the solar system, so if the NPA rotation was caused by cometary outgassing, it could still be in that state after cometary activity ceased. 1999 JM8's optical albedo is also consistent with the value of  $\sim 0.04$  estimated for comet Halley (Delamere *et al.*, 1986; Sagdeev *et al.*, 1986), although some comets have albedos as large as  $\sim 0.1$ .

However, no cometary activity was seen during the 1999 apparition despite extensive spectrophotometric observing

campaigns. The most reliable cometary radar albedo available is the estimate of  $\sim 0.04$  for IRAS-Araki-Alcock (Harmon *et al.*, 1989), a result that is comparable to our estimate for 1999 JM8. However, the nominal radar albedo of 1999 JM8 is also consistent with those estimated for primitive B-, F-, G-, and P-type main-belt asteroids (Magri *et al.*, 1999). The orbit of 1999 JM8 ( $a = 2.72 \text{ AU}$ ,  $e = 0.644$ ,  $i = 13.7^\circ$ ) has a Tisserand criterion = 2.988 that is consistent with an origin as a Jupiter-family comet. Still, many asteroids have comparable Tisserand values, so the Tisserand criterion is not compelling evidence for a cometary origin (Valsecchi *et al.*, 1995). Applying the Bottke *et al.* (2002) dynamical analysis to 1999 JM8, W. F. Bottke (pers. comm.) estimated a probability of  $\sim 8\%$  that 1999 JM8 is a Jupiter-family comet. Thus, although the evidence favors an origin as a primitive, outer main-belt asteroid, an origin as a comet nucleus cannot be excluded.

Given our images, it seems likely that inversion of the delay-Doppler images can improve constraints on the asteroid's shape significantly and define its spin state, following the example of 4179 Toutatis (Hudson and Ostro, 1995). The next radar opportunity is in 2008 when 1999 JM8 will approach within 0.315 AU of Earth. Estimated signal-to-noise ratios during that apparition could approach a few hundred per day and be adequate to refine the spin state.

*Acknowledgments*—Part of this research was conducted at the Jet Propulsion Laboratory, California Institute of Technology, under contract with the National Aeronautics and Space Administration (NASA). Work at Washington State University was supported, in part, by a grant from NASA. Some of the observations reported here were obtained with the Caltech Baseband Recorder (CBR), whose development and fabrication was funded by the National Science Foundation. The Arecibo Observatory is part of the National Astronomy and Ionosphere Center, which is operated by Cornell University under a cooperative agreement with the National Science Foundation and with support from NASA.

*Editorial handling:* W. Huebner

## REFERENCES

- ASPHAUG E. AND SCHEERES D. J. (1999) Deconstructing Castalia: Evaluating a post-impact state. *Icarus* **139**, 383–386.
- BELTON M. J. S. (1990) Rationalization of comet Halley's periods. *Icarus* **86**, 30–51.
- BELTON M. J. S., JULIAN W. H., ANDERSON A. J. AND MUELLER B. A. (1991) The spin state and homogeneity of comet Halley's nucleus. *Icarus* **93**, 183–193.
- BOTTKE W. F., MORBIDELLI A., JEDICKE R., PETIT J.-M., LEVISON H. F., MICHEL P. AND METCALFE T. S. (2002) Debaised orbital and absolute magnitude distribution of the near-Earth objects. *Icarus* (in press).
- CAMPBELL D. B., STACY N. J. S. AND HINE A. A. (1990) Venus: Crater distributions at low northern latitudes and in the southern hemisphere from new Arecibo observations. *Geophys. Res. Lett.* **17**, 1389–1392.
- DELAMERE W. A., REITSEMA H. J., HUEBNER W. F., SCHMIDT H. U., KELLER H. U., SCHMIDT W. K. H., WILHELM K. AND WHIPPLE F. L. (1986) Radiometric observations of the nucleus of comet Halley. In *20th ESLAB Symposium on the Exploration of Halley's*

- Comet* (eds. B. Battrick, E. J. Rolfe and R. Reinhard), pp. 355–357. ESA Special Publication 250, European Space Agency, Paris, France.
- GIBLIN I. AND FARINELLA P. (1997) Tumbling fragments from experiments simulating asteroid catastrophic disruption. *Icarus* 127, 424–430.
- HARMON J. K., CAMPBELL D. B., HINE A. A., SHAPIRO I. I. AND MARSDEN B. G. (1989) Radar observations of comet IRAS-Araki-Alcock 1983 d. *Astrophys. J.* 338, 1071–1093.
- HARRIS A. W. (1994) Tumbling asteroids. *Icarus* 107, 209–211.
- HARRIS A. W., YOUNG J. W., BOWELL E. AND THOLEN D. J. (1999) Asteroid lightcurve observations from 1981 to 1983. *Icarus* 142, 173–201.
- HUDSON R. S. AND OSTRO S. J. (1995) Shape and non-principal axis spin state of asteroid 4179 Toutatis. *Science* 270, 84–86.
- MAGRI C., OSTRO S. J., ROSEMA K. D., THOMAS M. L., MITCHELL D. L., CAMPBELL D. B., CHANDLER J. F., SHAPIRO I. I., GIORGINI J. D. AND YEOMANS D. K. (1999) Mainbelt asteroids: Results of Arecibo and Goldstone radar observations of 37 objects during 1980–1995. *Icarus* 140, 379–407.
- MOTTOLA S. A. ET AL. (1995) The slow rotation of 253 Mathilde. *Planet. Space Sci.* 43, 1609–1613.
- OSTRO S. J. ET AL. (1992) Europa, Ganymede, and Callisto: New radar results from Arecibo and Goldstone. *J. Geophys. Res.* 97, 18 227–18 244.
- OSTRO S. J. ET AL. (1996) Radar observations of asteroid 1620 Geographos. *Icarus* 121, 46–66.
- OSTRO S. J. ET AL. (1999) Asteroid 4179 Toutatis: 1996 radar observations. *Icarus* 137, 122–139.
- OSTRO S. J., HUDSON R. S., BENNER L. A. M., NOLAN M. C., MARGOT J.-L., GIORGINI J. D., JURGENS R. F., ROSE R. AND YEOMANS D. K. (2000) Radar observations of 4486 Mithra (abstract). *Bull. Am. Astron. Soc.* 32, 1003.
- OSTRO S. J., HUDSON R. S., BENNER L. A. M., NOLAN M. C., GIORGINI J. D., SCHEERES D. J., JURGENS R. F. AND ROSE R. (2001) Radar observations of asteroid 1998 ML14. *Meteorit. Planet. Sci.* 36, 1225–1236.
- PRAVEC P., ŠAROUNOVÁ L., BENNER L. A. M., OSTRO S. J., HICKS M. D., JURGENS R. F., GIORGINI J. D., SLADE M. A. AND YEOMANS D. K. (2000) Slowly rotating asteroid 1999 GU3. *Icarus* 148, 589–593.
- SAGDEEV R. Z., AVANESOV G. A., ZIMAN YA. L., SMITH B., TOTH I., MOROZ V. I., TARNOPOLSKY V. I., ZHUKOV B. S. AND SHAMIS V. A. (1986) TV experiment of the Vega mission: Photometry of the nucleus and inner coma. In *20th ESLAB Symposium on the Exploration of Halley's Comet* (eds. B. Battrick, E. J. Rolfe and R. Reinhard), pp. 317–326. ESA Special Publication 250, European Space Agency, Paris, France.
- SCHEERES D. J., OSTRO S. J., WERNER R. A., ASPHAUG E. AND HUDSON R. S. (2000) Effects of gravitational interactions on asteroid spin states. *Icarus* 147, 106–118.
- THOMPSON T. W., ZISK S. H., SHORTHILL R. W., SCHULTZ P. H. AND CUTTS J. A. (1981) Lunar craters with radar bright ejecta. *Icarus* 46, 201–225.
- VALSECCHI G. B., MORBIDELLI A., GONCZI R., FARINELLA P., FROESCHLE CH. AND FROESCHLE CL. (1995) The dynamics of objects in orbits resembling that of P/Encke. *Icarus* 118, 169–180.